Negative differential conductance and bistability in undoped GaAs/(Al,Ga)As quantum-cascade structures

S. L. Lu, L. Schrottke, S. W. Teitsworth,[a] R. Hey, and H. T. Grahn[b]
Paul-Drude-Institut für Festkörperelektronik, Hausvogteiplatz 5-7, 10117 Berlin, Germany

(Received 3 March 2006; accepted 10 April 2006; published online 17 July 2006)

We discuss the mechanisms for negative differential conductance (NDC) and bistable behavior observed in the current-density–electric-field (*j-F*) characteristics of undoped GaAs/$Al_{0.45}Ga_{0.55}As$ quantum-cascade structures (QCSs). While the *j-F* characteristic of a QCS with a single period exhibits NDC without bistability, NDC and a bistable behavior are observed for a QCS with 20 periods of the same design. Calculations using a scattering-rate model neglecting any field inhomogeneities show that the interplay of resonant tunneling between the states in the QCS with resonant scattering of longitudinal optical phonons can lead to NDC in both structures. However, the bistable behavior in the QCS with 20 periods can only be explained if an inhomogeneous field distribution due to charge accumulation is taken into account in addition to the NDC. The abrupt decrease of the current density at the field strength of the bistability is attributed to a rapid decrease of the accumulated charge, which is confirmed by electric-field-dependent photoluminescence spectroscopy. © *2006 American Institute of Physics*. [DOI: 10.1063/1.2214362]

I. INTRODUCTION

Quantum-cascade lasers (QCLs) based on GaAs/(Al,Ga)As heterostructures grown on GaAs substrates are now used for solid-state infrared lasers,[1–5] in particular, for longer wavelengths (terahertz radiation).[6] While the basic principles of their operation are well understood, the variation of the lasing energies of nominally identical QCLs (Ref. 7) as well as rather large threshold current densities for the GaAs/(Al,Ga)As materials system require additional investigations.

Due to the complex structure of the basic unit of QCLs, a detailed experimental investigation of the individual underlying processes such as carrier transport and subband population as well as a complete theoretical description are challenging. In particular, the correlation of theoretical predictions with experimental results may sometimes be ambiguous, since the developed theoretical models[8,9] need a large number of parameters and have to be compared with experimental data, which are often restricted to current-voltage and light-current characteristics. Already the operating field strength can only be approximately determined from the applied voltage, since the differential conductance of the cascade structure is strongly nonlinear, while it is more or less constant for the contact and waveguide layers. It may even be possible that, at the operating field strength of the laser, the differential conductance of the cascade is larger than the one of the contact and waveguide layers. In contrast, the lasing energies and threshold current densities can be rather accurately determined. In view of the restricted experimental data, a simplification of the theoretical models appears to be appropriate, if these are closely correlated with experimental results. Even the qualitative discussion of pronounced experimental features can provide further insight into the operation mechanisms of QCLs.

The formation of electric-field domains in doped quantum-cascade structures (QCSs) below threshold[10] has been recently investigated applying a scattering-rate approach in the framework of the self-consistent solution of the Schrödinger and Poisson equations considering only scattering between subbands at $\boldsymbol{k}=0$ and neglecting in-plane *k*-space integration as described in detail in Ref. 11. The formation of global field domains, i.e., a spatial electric-field distribution spanning the entire QCS, in which a single low-field and a single high-field domain are separated by a charge accumulation layer, in such structures is affected by the presence of local field domains, i.e., specific forms of an electric-field inhomogeneity that occur identically within each period of the QCS.[12] In particular, the local field domains will influence the resonant tunneling condition. In addition, the impact of the operating field strength on the lasing properties of GaAs/(Al,Ga)As QCLs has been analyzed using the same model.[11]

We focus on the transport properties of undoped QCSs, in particular, on the appearance of negative differential conductance (NDC) and bistability. The population inversion in QCLs is usually achieved by resonant coupling between an injector state and the upper laser level, which can result in NDC. Recently, the existence of several regions of NDC was reported for undoped GaAs/$Al_xGa_{1-x}As$ QCSs with $x=0.33$ and 0.45.[13] It was theoretically predicted that NDC related to the resonant coupling between the injector and upper laser level may be found for QCSs with $x=0.45$, but not in QCSs with $x=0.33$,[8] which was confirmed by the observation of a smooth type of NDC without any bistability for QCSs with $x=0.45$. In contrast, a pronounced bistable current-density–electric-field (*j-F*) characteristic has been observed for QCSs of both Al compositions typically used, which appears at

[a]Permanent address: Department of Physics, Duke University, Box 90305, Durham, North Carolina 27708-0305.
[b]Electronic mail: htgrahn@pdi-berlin.de

smaller field strengths than the smooth NDC region. In addition, an abrupt change of the photoluminescence (PL) intensity as well as the PL energy positions was observed at the critical field strength F_{crit} for the bistable behavior, which suggested that the bistability may be caused by an interplay of resonant coupling effects within the injector with field inhomogeneities due to charge accumulation. However, the underlying process was not identified.

In this paper, we discuss the connection between NDC and bistability for undoped QCSs. For a $GaAs/Al_{0.45}Ga_{0.55}As$ QCS with 20 periods, the formation of the bistability is a consequence of an abrupt change in the distribution of the accumulated charge, which is correlated with the NDC because of current conservation. Since the subband structure of the QCS suggests that the NDC is caused by an interplay of resonant coupling between the ground state in the active region and injector states with the resonance of the intersubband transitions with longitudinal optical (LO) phonons, we apply the scattering-rate model outlined in Ref. 11 to undoped QCSs. In order to confirm the results of this model, we also investigated the transport properties of the same $GaAs/Al_{0.45}Ga_{0.55}As$ QCS containing only one single period without the influence of global field inhomogeneities. This structure exhibits only a smooth NDC region without any bistability.

II. EXPERIMENTAL DETAILS

Two undoped $GaAs/Al_{0.45}Ga_{0.55}As$ QCSs based on the design of Page *et al.*[2] were grown by molecular-beam epitaxy on GaAs(100) substrates. Samples A and B contain the same layer sequence for each period, which is, starting with the injection barrier, **4.6**, 1.9, **1.1**, 5.4, **1.1**, 4.8, **2.8**, 3.4, **1.7**, 3.0, **1.8**, 2.8, **2.0**, 3.0, **2.6**, and 3.0 nm (bold numbers indicate barriers). Sample A consists of 20 periods, while sample B contains only a single period. The cladding layers are replaced by 400-nm-thick n^+-GaAs contact layers in order to reduce a large voltage drop over the weakly doped waveguide layers. Both samples were processed into mesa structures with metal contacts on top. In order to allow for optical access, the top contact is a ring contact providing a window for optical excitation as well as PL detection. For the optical measurement, we used the anti-Stokes configuration, i.e., carriers are only excited in the contact layers with an excitation energy of about 1.53 eV. The excitation power was varied between 2 and 220 μW. A more detailed description of the experimental techniques for the transport and PL measurements can be found in Refs. 13 and 14.

III. THEORETICAL MODEL

The model is based on the Schrödinger equation in the envelope function approximation. In order to incorporate the nonparabolicity of the band structure, an effective mass, which depends linearly on energy, is used.[15] The resulting quasi-$\boldsymbol{k}\cdot\boldsymbol{p}$ model with two bands is solved numerically by means of Fourier analysis using standard numerical routines. The carrier distribution is determined in the framework of a simple rate-equation model with periodic boundary conditions. For this calculation, the heterostructure is assumed to be infinite, and all periods of the structure are equal. For simplicity, k-space integration is neglected, and the transport is described using scattering rates, which are assumed to be proportional to the corresponding dipole matrix element D_{mn} for a respective pair of states determined according to Ref. 16. In order to simulate the in-plane k-space integration, the transition rates T_{mn} depend also on the transition energies $\Delta E=E_m-E_n$, so that we use for the numerical simulation $T_{mn}=\tau(\Delta E)|D_{mn}|^2$ with an energy-dependent factor $\tau(\Delta E)$. LO-phonon scattering is simulated by a steplike increase of $\tau(\Delta E)$ for energies around the LO-phonon energy $\hbar\omega_{LO}$ of GaAs (36 meV) with a superposition of a Lorentzian line shape. For thermal activation of carriers, an exponentially decaying contribution is allowed. To calculate the current density j, we sum over all carrier transitions of one period into the next one through any interface determined by $N_m T_{mn}$, i.e., by the product of the transition rate and the population of the respective initial state. A detailed description of the model including the full set of equations can be found in Ref. 11.

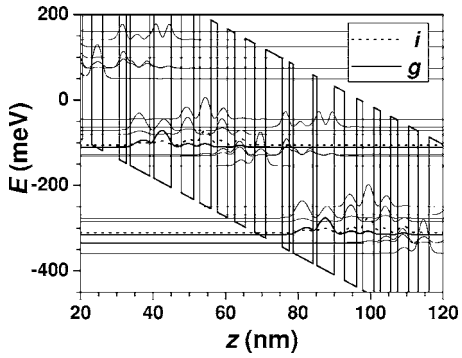

FIG. 1. Calculated conduction band profile, energy levels, and electron probability density at $F=45.5$ kV/cm for the structure of sample A neglecting field inhomogeneities. The ground state g in the active region and the intermediate injector state i are marked by the thick solid and dotted lines, respectively.

Figure 1 shows the calculated conduction band profile, energy levels, and electron probability density for an electric-field strength F of 45.5 kV/cm for the structure of sample A. This field strength is in close proximity to F_{crit} at which the bistability is observed in this structure. For $F=45.5$ kV/cm, the ground state g in the active region couples resonantly to an intermediate injector state i. At the same time, the energy difference between the lower laser level and g as well as between i and the injector ground state is comparable to the LO-phonon energy in GaAs so that an enhanced transport probability is expected.

Figure 2 shows the calculated j-F curves without and with taking into account LO-phonon scattering in the simulation, which only gives values for j in arbitrary units. The effect of the LO-phonon scattering can be simply switched on or off by the appropriate choice of $\tau(\Delta E)$. In the case of a constant $\tau(\Delta E)$, i.e., without LO-phonon coupling, the j-F characteristic shows basically a monotonic, exponential-like increase, while in the case of a steplike increase of $\tau(\Delta E)$ at $\hbar\omega_{LO}$, i.e., with LO-phonon coupling, there is a pronounced enhancement of j for field strengths between 25 and 55 kV/cm with a maximum at about 45.5 kV/cm. In addi-

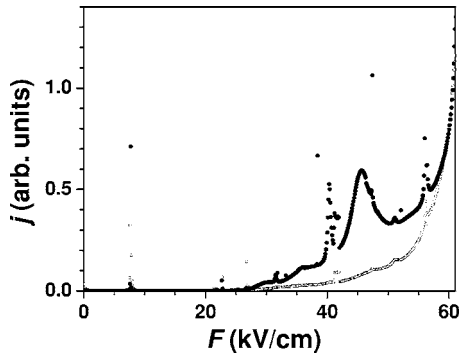

FIG. 2. Calculated *j-F* characteristics for the structure of sample A neglecting field inhomogeneities without (circles) and with taking into account LO-phonon scattering (dots). The current density calculated without LO-phonon scattering has been multiplied by a factor of 12.

tion, in both cases several very sharp resonances appear due to resonant coupling of several pairs of subband states in the cascade, because we have neglected level broadening, field inhomogeneities, and interface roughness. In contrast to the broad maximum at 45.5 kV/cm, these sharp resonances are present independently of whether the LO-phonon scattering is switched on or off. We interpret the appearance of the broad maximum as an interplay of the LO-phonon resonance in the transport characteristics with the resonant coupling of particular subbands, namely, *g* and *i*. In the absence of the phonon resonance, the coupling of all subbands in the cascade structures would average out leading to the rather monotonically increasing *j-F* curve without any broad maximum.

The N-shape NDC shown in Fig. 2 for the case of LO-phonon coupling may result in a bistable behavior, if a current-limiting process is present. A connection of the QCS with a sufficiently large Ohmic resistor in series can convert the N-shape *j-F* curve of the cascade into a bistable characteristic for the complete sample including the contact layers. Close to the maximum of the N-shape *j-F* curve, the voltage drop over the contact also reaches a maximum value, while in the decreasing part of the *j-F* curve the voltage drop over the contact decreases. Consequently, for a fixed current value in the NDC region, the total applied voltage can decrease, leading to a bistability.

The calculated *j-F* curve shown in Fig. 2 reflects, strictly speaking, the relationship between an effective drift velocity v and the electric-field strength F for a single period. However, it is only valid for a homogeneous field distribution. Carrier injection from the contact layers may inevitably induce a charge accumulation inside the structure and subsequently an inhomogeneous distribution of the electric field as discussed in Ref. 17 for QCLs. In order to determine whether such inhomogeneities can result in a bistability, we consider for simplicity the *v-F* characteristics as a local property, i.e., we consider $v[F(z)]$, where z denotes the growth direction. In this case, the relation between F, j, and the distribution of the carrier density $n(z)$ is given by the following equations:

$$n(z) = \frac{\epsilon_0 \epsilon}{e} \frac{dF(z)}{dz} \tag{1}$$

and

$$j = en(z)v[F(z)] = \epsilon_0 \epsilon \frac{dF(z)}{dz} v[F(z)], \tag{2}$$

where ϵ_0 denotes the dielectric permittivity of the vacuum, ϵ the dielectric constant of the material, and e the elementary charge. Applying current conservation, we can rewrite Eq. (2) in the following way:

$$jdz = \epsilon_0 \epsilon v[F(z)]dF(z). \tag{3}$$

For a complete determination of the solution, we would also have to specify boundary conditions (see Ref. 18). However, we can use these equations for a qualitative discussion. Since the system is unipolar, i.e., $n(z)$ does not change its sign, $F(z)$ is monotonic. Furthermore, $v[F(z)]$ is always positive. Therefore, there is a unique solution for $F(z)$ using the boundary condition for the applied voltage $U_0 = \int_0^l F(z)dz$ for any $|F(0)| \leq |U_0|/l$, i.e., we do not expect a bistability that is intrinsic to the QCS by itself. The actual values for $F(0)$ and the total injected charge q per unit area $[=e\int_0^l n(z)dz]$ cannot be determined from this system of equations, since they will depend on the specific properties of the transition region between the contact layer and the first period of the QCS as well as on $F(0)$ itself. Nevertheless, there is clear correlation between q and $F(0)$, i.e., a larger value of q will increase the bowing of $F(z)$ and consequently decrease $F(0)$.

The formation of the bistability may be qualitatively explained by an interplay of a small voltage drop over the contact layer and a charging of the (undoped) QCS. In the NDC regime, periods of the cascade experiencing larger field strengths (i.e., closer to the anode) exhibit a smaller value of v. In order to conserve the current, the charge density $en(z)$ in these regions must increase, which may result in a smaller increase of the voltage drop over the cascade and a comparatively larger increase of the voltage drop over the contacts, when the total applied voltage is increased. In this situation, the carrier density at the cathode may be smaller than the carrier density at the anode. As a result, the bowing of $F(z)$ is reduced at the cathode, but the field strength at the cathode $F(0)$ may increase so that the total charge q becomes larger. For higher applied voltages, when the regions at the anode reach normal conductance, this recharging will be reversed again, i.e., the extra charge close to the anode can flow out. This discharging may lead to a smaller total charge q and a larger voltage drop over the entire cascade and, hence, a larger average internal field strength, resulting in a positive feedback for this process. If the value of the injected charge, the injection characteristics of the contacts, and the shape of the NDC result in a positive feedback, this situation may be characterized by a bistable behavior.

IV. RESULTS AND DISCUSSION

Figure 3(a) shows the *j-F* characteristics of sample A for two different mesa sizes recorded at 6 K without any laser illumination. As already reported in Ref. 13, a pronounced bistability appears at about 49 kV/cm. The second, weak NDC at about 55 kV/cm is interpreted to be due to the resonant coupling between the upper laser level and the adjacent, upstream injector state. Figure 3(b) presents the *j-F* charac-

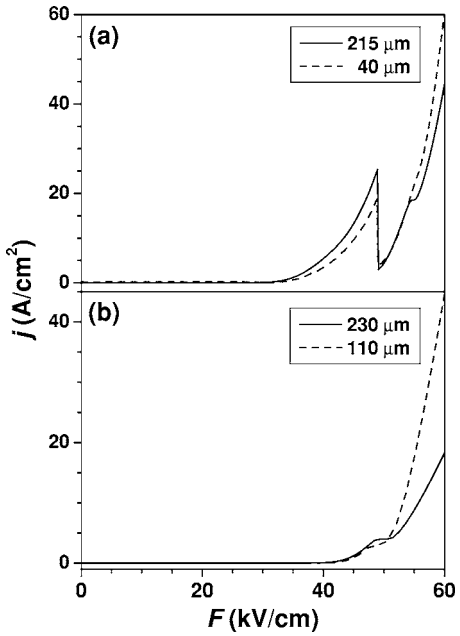

FIG. 3. Measured *j-F* characteristics of (a) sample A for mesa diameters of 215 μm (solid line) and 40 μm (dashed line) as well as (b) sample B for mesa diameters of 230 μm (solid line) and 110 μm (dashed line) at 6 K. The field strength *F* was determined from the applied voltage divided by the thickness of 950 nm for sample A and 95 nm for sample B neglecting the contact layers.

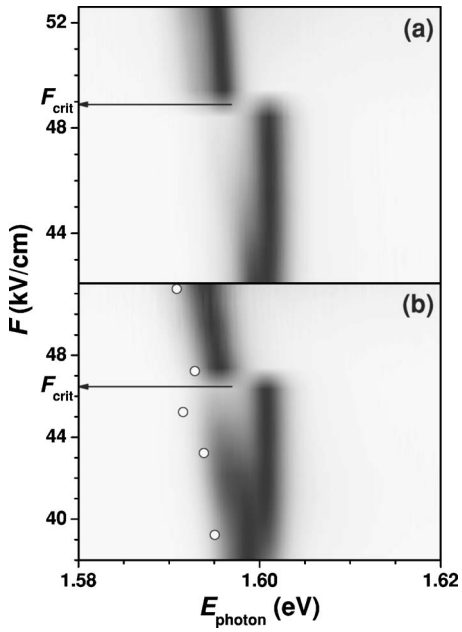

FIG. 4. Normalized anti-Stokes PL spectra of sample A vs electric field *F* and detection energy E_{photon} in a grey scale presentation for (a) $P_{\text{exc}}=2$ μW and (b) $P_{\text{exc}}=220$ μW with $\lambda_{\text{exc}}=810$ nm ($E_{\text{exc}}=1.53$ eV) at 6 K. The arrows indicate the critical field strength F_{crit}, where bistable behavior is observed. For comparison, the circles indicating the calculated transition energies for the ground state are added in (b).

teristics of sample B for two different mesa sizes at 6 K. Sample B contains only one period so that global field inhomogeneities cannot exist. In addition, since there is no resonant coupling of a preceding injector with the upper laser level, the second, weak NDC does not appear. At about 48 kV/cm, the *j-F* curve exhibits a smooth NDC regime, but without any bistability for both mesa sizes. Furthermore, there is no second NDC region as expected. For both samples, the electric-field strength was determined by dividing the applied voltage by the thickness of the cascade structure including the spacer layers, but without the contact layers. The contact resistance was estimated to be between 1 and 2 Ω, so that it can be neglected. However, it is more than one order of magnitude smaller than the necessary value for obtaining a bistable behavior by considering only the connection of the QCS with an Ohmic resistor in series. In Ref. 13, we excluded the possibility that the first few layers of the first period of the cascade structure alone can cause the bistability. In addition to that, the *j-F* characteristic of sample B suggests that the first period after the contact layer alone will not lead to a bistable behavior. The similarity of the *j-F* characteristics close to the NDC regime for different mesa sizes also excludes effects of the external circuit on the bistability as discussed by Sollner[19] and Foster *et al.*[20] for double-barrier resonant tunneling diodes. In that case, bistability is merely caused by the current oscillations in the device and external circuit.

We believe that the NDC present in the *j-F* characteristic of sample B can be explained by our simple scattering-rate approach, since the field strength at which NDC is observed agrees with the respective field strength in the calculated characteristic. This result confirms our assumption that the interplay of resonant tunneling with LO-phonon scattering can lead to NDC in undoped QCL structures. Note that there is a similarity with the formation of electric-field domains in doped QCLs insofar as the resonant coupling of the state *g* with different injector states *i* plays an important role for the high-field domain as discussed in Ref. 10. In the doped structures, however, the influence of this resonance is affected by the local field domains rather than by the LO-phonon coupling as in the present case.

In order to confirm our model, we need to investigate the carrier distribution inside the cascade structure. Unfortunately, the carrier density cannot be measured directly. However, PL spectroscopy has been shown to be an appropriate tool to determine the electron population and distribution in QCSs.[14] Figures 4(a) and 4(b) show the anti-Stokes PL spectra of the conduction band ground state and the lower laser level of sample A for different electric-field strengths in a grey scale presentation for excitation powers of 2 and 220 μW, respectively. The arrows indicate the critical field strength F_{crit}, for which the bistable behavior is observed in the *j-F* characteristic. F_{crit} depends on the excitation density, i.e., it decreases with increasing laser power. This observation agrees with previous measurements of the power density dependence of the *j-F* characteristics.[13]

For low excitation power [see Fig. 4(a)], the PL energy of the observed peak exhibits an abrupt shift of about 5 meV to lower values at F_{crit}. At the same time, the PL intensity is strongly quenched above F_{crit}, which cannot be seen in Fig. 4(a) due to the presentation of normalized PL spectra. An abrupt shift of the PL energy and a strong quenching of the PL intensity have been observed as well for a number of QCSs with both $Al_{0.45}Ga_{0.55}As$ and $Al_{0.33}Ga_{0.67}As$ barriers.

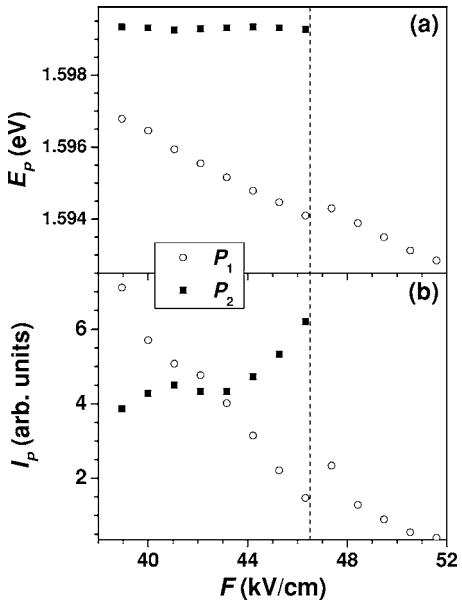

FIG. 5. (a) PL peak energies E_P and (b) integrated PL intensities I_P of the lower-energy peak P_1 (circles) and the higher-energy peak P_2 (squares) of the spectra shown in Fig. 4(b) as a function of electric field F. The energies and integrated intensities were obtained by fitting the spectra to two Lorentzians. The vertical dashed line indicates the critical field strength F_{crit}, where bistable behavior is observed.

For higher excitation powers [see Fig. 4(b)], a splitting of the PL line is observed below F_{crit} so that the main PL peak is divided into two. The lower-energy peak P_1 exhibits a redshift, while the position of the one at higher energies P_2 remains unchanged with increasing electric field. For comparison, the calculated transition energies for the ground state in the widest quantum well in the active region are also included in Fig. 4(b) marked as circles, showing a redshift with increasing electric-field strength similar to the behavior of P_1.

Figures 5(a) and 5(b) display the electric-field dependence of the PL peak energy E_P and the integrated PL intensities I_P, respectively, of the two peaks P_1 and P_2 obtained by fitting two Lorentzians for $F<F_{\mathrm{crit}}$ and one Lorentzian for $F>F_{\mathrm{crit}}$ to the spectra shown in Fig. 4(b). The increase of the electric-field strength leads to a decrease of the PL intensity of P_1 and an increase of the one for P_2. The peak P_2 does not change its energy with increasing applied field. Both peaks P_1 and P_2 are assigned to the ground-state transition in the widest quantum well, but for periods experiencing different field strengths. Note that for low excitation powers and above F_{crit}, only a single peak is visible. The calculated values in Fig. 4(b) have been obtained using an average electric field.

The largest hole concentration is expected in the vicinity of the anode (bottom contact), since in the anti-Stokes case electrons and holes are only excited in the contact layers. However, close to the anode, the inhomogeneous field distribution should result in the largest field value, so that the holes are probably transferred rather quickly from the anode into several periods of the cascade structure that are adjacent to the anode. For a detailed discussion of the carrier distribution, a simultaneous calculation of the electron and hole distribution through the entire structure taking into account the contact properties is necessary, which is beyond the capabilities of our numerical procedure. Therefore, at this point, only a qualitative discussion is possible.

In view of our theoretical consideration, we assume an increased electron concentration in those periods, in which the local field strength corresponds to the negative differential velocity (NDV) region of the (intrinsic) $v-F$ curve. Below F_{crit}, increasing the applied field will result in an increase of the accumulated charge. Consequently, the PL intensity of P_2 increases, and, at the same time, the field inhomogeneity is enhanced so that the difference between the energies of P_1 and P_2 also increases. Assuming that the charge accumulation is related to the NDV region, the field strength in the vicinity of the accumulated charge should be constant. As a result, the energy of P_2 remains unchanged. At F_{crit}, when the current switches to its lower value, the accumulated charge is spread out, and, consequently, the field inhomogeneity is significantly reduced. Therefore, the PL spectra related to the ground state transition are dominated above F_{crit} by one peak with an energy corresponding to the average electric-field strength. The appearance and disappearance of P_2 are a result of the accumulation and dissipation of the space-charge layer. Furthermore, the minimum current density at F_{crit} is for both samples almost identical (see Fig. 3). This observation is another confirmation for our interpretation that the bistable behavior of sample A is induced by the rapid dissipation of the space-charge layer, which appears due to NDC in QCSs with a homogeneous field distribution.

Using this interpretation, we can also understand the carrier-density dependence of the *j-F* characteristics in undoped QCS as reported in Ref. 13. With increasing excitation density, the increasing density of photoexcited holes may screen the charge accumulation layer that is related to the bistability. Therefore, the peak-to-valley ratio of the current density is reduced due to the decrease of feedback of the space charge with the field. However, when the electron density inside the structure is sufficiently large, a plateaulike structure is formed in a similar way as discussed in Ref. 10, so that the interplay of the resonant coupling of subbands with local field inhomogeneities inside each period dominates over the mechanism that relies on resonant LO-phonon coupling.

V. CONCLUSIONS

We have discussed a possible mechanism for the manifestation of NDC and bistable behavior in the *j-F* characteristics of undoped quantum-cascade structures. We attribute the appearance of the NDC to an interplay of resonant tunneling between different subbands with resonant LO-phonon scattering. This conclusion was derived from a comparison of the *j-F* characteristic calculated in the framework of a scattering-rate approach with the experimentally observed *j-F* characteristic for a QCS containing only a single period. For a multiperiod QCS, the bistable behavior is assigned to the electric feedback of the appearance and disappearance of

a charge accumulation layer, which is connected with the simultaneous appearance of NDC and an inhomogeneous field distribution.

ACKNOWLEDGMENTS

The authors would like to thank H. Kostial and E. Wiebicke for sample processing.

[1]C. Sirtori, P. Kruck, S. Barbieri, P. Collot, J. Nagle, M. Beck, J. Faist, and U. Oesterle, Appl. Phys. Lett. **73**, 3486 (1998).
[2]H. Page, C. Becker, A. Robertson, G. Glastre, V. Ortiz, and C. Sirtori, Appl. Phys. Lett. **78**, 3529 (2001).
[3]L. R. Wilson, P. T. Keightley, J. W. Cockburn, M. S. Skolnick, J. C. Clark, R. Grey, and G. Hill, Appl. Phys. Lett. **76**, 801 (2000).
[4]D. Indjin, S. Tomić, Z. Ikonić, P. Harrison, R. W. Kelsall, V. Milanović, and S. Kočinac, Appl. Phys. Lett. **81**, 2163 (2002).
[5]S. Anders, W. Schrenk, E. Gornik, and G. Strasser, Appl. Phys. Lett. **80**, 1864 (2002).
[6]R. Köhler *et al.*, Nature (London) **417**, 156 (2002).
[7]M. Giehler, R. Hey, H. Kostial, S. Cronenberg, T. Ohtsuka, L. Schrottke, and H. T. Grahn, Appl. Phys. Lett. **82**, 671 (2003).
[8]S.-C. Lee and A. Wacker, Phys. Rev. B **66**, 245314 (2002).
[9]R. C. Iotti and F. Rossi, Phys. Rev. Lett. **87**, 146603 (2001).
[10]S. L. Lu, L. Schrottke, S. Teitsworth, R. Hey, and H. T. Grahn, Phys. Rev. B **73**, 033311 (2006).
[11]L. Schrottke, M. Giehler, R. Hey, and H. T. Grahn, J. Appl. Phys. (submitted).
[12]V. D. Jovanović *et al.*, Appl. Phys. Lett. **86**, 211117 (2005).
[13]S. L. Lu, L. Schrottke, R. Hey, H. Kostial, and H. T. Grahn, J. Appl. Phys. **97**, 024511 (2005).
[14]L. Schrottke, R. Hey, and H. T. Grahn, Appl. Phys. Lett. **84**, 4535 (2004).
[15]See, e. g., G. Bastard, *Wave Mechanics Applied to Semiconductor Heterostructures* (Les éditions de physique, Les Ulis, 1988), pp. 83–89.
[16]C. Sirtori, F. Capasso, J. Faist, and S. Scandolo, Phys. Rev. B **50**, 8663 (1994).
[17]C. Sirtori, F. Capasso, J. Faist, A. L. Hutchinson, D. L. Sivco, and A. Y. Cho, IEEE J. Quantum Electron. **34**, 1722 (1998).
[18]L. L. Bonilla and H. T. Grahn, Rep. Prog. Phys. **68**, 577 (2005).
[19]T. C. L. G. Sollner, Phys. Rev. Lett. **59**, 1622 (1987).
[20]T. J. Foster *et al.*, Phys. Rev. B **39**, 6205 (1989).